Available online at www.sciencedirect.com
ScienceDirect
Journal of Nuclear Materials 376 (2008) 47–59
journal of nuclear materials
www.elsevier.com/locate/jnucmat

AC-3-irradiation test of sphere-pac and pellet (U,Pu)C fuel in the US Fast Flux Test Facility

G. Bart [a,*], F.B. Botta [a,b,c,1], C.W. Hoth [b], G. Ledergerber [c], R.E. Mason [b], R.W. Stratton [a,b,c,1]

[a] *Paul Scherrer Institute, 5232 Villigen PSI, Switzerland*
[b] *LANL, Los Alamos, USA*
[c] *KKL, Leibstadt, Switzerland*

Received 6 September 2007; accepted 29 January 2008

Abstract

The objective of the AC-3 bundle experiment in the Fast Flux Test Facility (FFTF) was to evaluate a fuel fabrication method by 'direct conversion' of nitrate solutions into spherical uranium–plutonium carbide particles and to compare the irradiation performance of 'sphere-pac' fuel pins prepared at Paul Scherrer Institute (PSI) with standard pellet fuel pins fabricated at Los Alamos National Laboratory (LANL). The irradiation and post test examination results show that mixed carbide pellet fuel produced by powder methods and sphere-pac particle fuel developed by internal gelation techniques are both valuable advanced fuel candidates for liquid metal reactors. The PSI fabrication process with direct conversion of actinide nitrate solutions into various sizes of fuel spheres by internal gelation and direct filling of spheres into cladding tubes is seen as more easily transferable to remote operation, showing a significant reduction of process steps. The process is also adaptable for the fabrication of carbonitrides and nitrides (still based on a uranium matrix), as well as for actinides diluted in a (uranium-free) yttrium stabilized zirconium oxide matrix. The AC-3 fuel bundle was irradiated in the Fast Flux Test Facility (FFTF) during the years 1986–1988 for 630 full power days to a peak burn up of ~8 at.% fissile material. All of the pins, irradiated at linear powers of up to 84 kW/m, with cladding outer temperatures of 465 °C appeared to be in good condition when removed from the assembly. The rebirth of interest for fast reactor systems motivated the earlier teams to report about the excellent, still perfectly relevant results reached; this paper focusing on the sphere-pac fuel behaviour.

1. Introduction

From the early stages of fast breeder reactor development, carbide ceramics were recognized as candidate fuels for Liquid Metal Fast Breeder Reactors (LMFBR) with advantages over the standard oxide fuel form [1]. As a dense material like nitrides and carbonitrides they reveal a high thermal conductivity, melting point and a high heavy metal atomic density. These properties enable carbide fuels to operate at high linear power rates (80 kW/m) and with high breeding gains.

The potential limitations on the use of carbide, nitride and carbonitride fuel are the somewhat more complex fabrication processes than for oxides, the eventual fuel swelling [2], the potential carburisation of the cladding and the more difficult fuel dissolution after irradiation which complicates the established aqueous reprocessing. This latter concern is studied with success by the Indira Gandhi Centre for Atomic Research (IGCAR) at Kalpakkam [3,4].

To evaluate the above mentioned pros and cons and in order to compare the advantages/disadvantages of pellet- vs. sphere-pac fuel, LANL, which was highly experienced in testing pellet type carbide fuel in the EBR-II reactor [1] and PSI with its expertise in preparing and irradiating sphere-pac carbide fuel by internal gelation [5], installed a cooperation agreement during the 70s and tested a full fuel

* Corresponding author.
E-mail address: gerhard.bart@psi.ch (G. Bart).
[1] Retired.

0022-3115/$ - see front matter © 2008 Elsevier B.V. All rights reserved.
doi:10.1016/j.jnucmat.2008.01.022

assembly of 91 mixed carbide pins at the Fast Flux Test Facility in Hanford, USA, during 1986–1988. The irradiation, which was conservatively based on experience from earlier mixed carbide irradiation tests made on pellet pins in EBR-II [6–8], and on sphere-pac pins in several European reactors [9–11] was successful, none of the pins failed but the irradiation was stopped early due to political decisions concerning the FFTF installation and the US FBR fuel research program. Post irradiation examination (PIE) was performed between 1989-1991 at WHE, Hanford, in the Hot Fuels Examination Facility (HFEF), Idaho, and at ANL, Chicago. [12]. Analysis and reporting of the AC-3 bundle irradiation behaviour were performed by LANL and PSI. With decreasing interests in FBR fuels both on the US and Swiss side, the successful program was not finished with a public final report.

Due to the worldwide renewed strong interest in advanced, fast reactor systems, demonstrated with the US 'Global Nuclear Energy Partnership' (GNEP) and 'Generation IV International Forum' (GIF) initiatives and the participation of Switzerland in GIF, this situation changed and the motivation was given for LANL and PSI to finalize the reporting on the successful, perfectly relevant AC-3 carbide irradiation program.

2. Carbide sphere-pac fuel advantages and AC-3 fuel design

The use of advanced, dense nitride-, carbide- or metallic fuel with high thermal conductivity in a small core would reduce the time needed to breed extra plutonium by nearly a factor of two compared to mixed oxide, which is the proven FBR fuel with rather low breeding ratio [1,13]. However carbide fuels are somewhat difficult to fabricate on a large scale since they are pyrophoric and susceptible to oxidation and hydrolysis. Also reprocessing of the spent carbide fuel is complicated as it is difficult to dissolve carbides in nitric acid, which leads to the formation of organic complexes hampering the subsequent actinide extraction process. If the carbides are first converted into oxides or nitrides one still has to deal with carbon particles left over in the dissolver bath. Nevertheless these problems can successfully be overcome [3].

Concerning the geometrical fuel form, closing the fuel cycle asks for simple, economic, proliferation resistant, radiologically- and criticality-safe fuel production steps, be it for homogeneous or heterogeneous recycling of actinides. These aspects call for low decontaminated, remotely processed actinide containing fuel, extracted from reprocessing. Particle fuels gained from dry, salt-melt electrowinning or from internal gelation processes might, for these purposes, be excellent alternatives to the common well established powder/pellet fuel production technology [14]. Compared to the pellet fuel preparation scheme, including several blending steps and leading to a certain fuel inhomogeneity, the internal gelation fuel production is nearly dust-free and provides a ceramic with perfect homogenisation of Pu and U on atomic scale. Also, starting with varying liquid admixtures and altering the heat treatment environments, carbides as well as oxides and nitrides with varying amounts of added Minor Actinides (MA) can be produced [15]. To cope for Am sintering losses, the fuel particle sinter temperatures of 1920 °C applied for the AC-3 test would have to be reduced significantly though [16]. The sol–gel process with subsequent direct thermal treatment reduces the number of fabrication steps and (in parallel) the fuel production costs (Fig. 1). Thus being simpler than a dry standard pellet fabrication process, the remotely controllable internal gelation fuel fabrication process, allowing the treatment of low decontaminated and MA- containing U–Pu liquors (needing significantly less processing space) could be attractive for FBR- on site fuel cycle closure.

2.1. Sphere-pac fuel production

The AC-3 sol–gel fuel process starts with acid free, concentrated feed solutions of uranium and plutonium nitrates, which were mixed together with an aqueous solution of hexamethylenetetramine (HMTA), urea and dis-

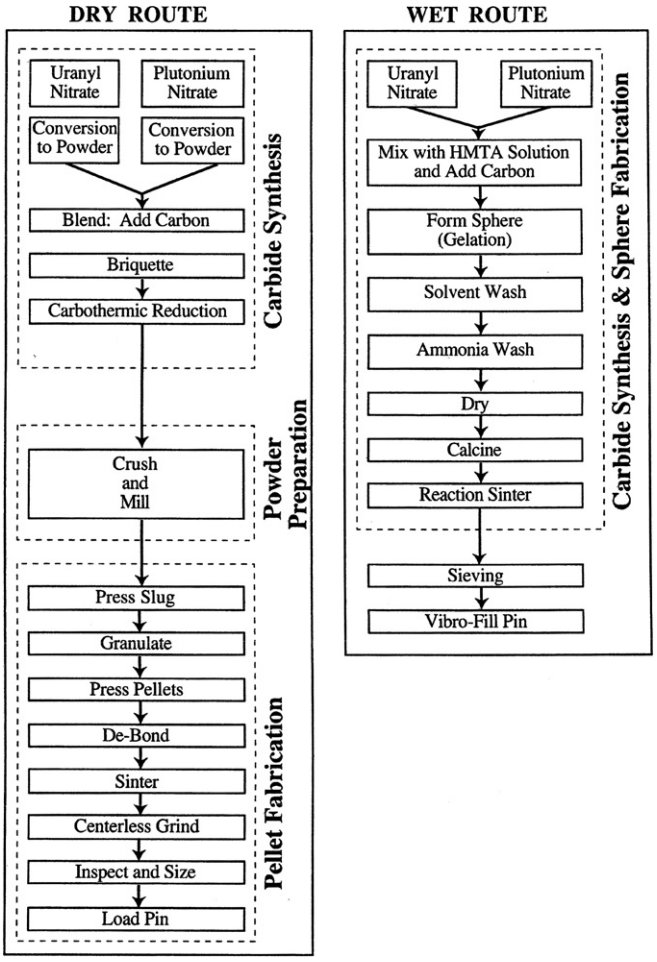

Fig. 1. Schematic diagram of AC-3 sphere-pac vs. pellet pin design.

persed carbon black (Fig. 1). This mixture was cooled and dropped into a column of hot silicon oil (to prepare sintered particles of ~800 μm in diameter) or injected into a stream of hot oil (for small ~80 μm fuel particles). The temperature rise in the droplets leads to the decomposition of the HMTA and urea to form ammonia; this in turn precipitates ammonium-diuranate and -plutonate within the droplets, forming solid spheres which can readily be handled when arriving at the bottom of the oil filled column. Washing with solvents removed the silicon oil and reaction products and, after drying at 110 °C in air, the particles were calcined for 6 h at 700 °C in argon/hydrogen environment to the oxidation state of $(U,Pu)O_2$. The last step consisted in the reaction-sintering at 1950 °C in flowing argon for 8 h, which produced clean, dust-free spherical particles with >95% theoretical density (TD), which could then be loaded directly into fuel pins. As indicated before, two size fractions of fuel particles of 630-900 μm and 45–106 μm diameter were used to reach the required AC-3 smeared densities of approximately 80%TD [17].

Due to criticality limits for the individual glove boxes (200 g plutonium) and the limited capacity of the sinter oven, production was broken down into small batches containing 70 g of plutonium each. Each batch started from a single make up of feed solutions (metal- and HMTA-solutions) and proceeded through the gelation, drying, calcining and sintering steps. Carbon, oxygen and plutonium analyses were performed and ceramographic specimens prepared to qualify each batch. A charge consisting of fuel of one fraction for approximately five pins was prepared which meant some 2 kg (U,Pu)C of large and 750 g (U,Pu)C of fine spheres. The individual fuel batches and fuel charges showed excellent chemical reproducibility for the major-, minor-, and trace element- fuel components, except for tungsten and (in one case) for silicon (Table 1). The scatter of tungsten and silicon were due to the application of tungsten sintering crucibles and an incomplete silicon washing process. The micro-spheres showed a two-phase composition. The matrix phase was monocarbide (U,Pu)C. The identity of the secondary phase remained uncertain. Neutron diffractrometry suggested that it was a nascent dicarbide – nearly amorphous; of very small crystallite size. It was readily transformed into sesquicarbide $(U,Pu)_2C_3$ by an extra annealing thermal treatment at 1435-1500 °C for as little as 2 hours [5].

2.2. Pellet fuel production

The fabrication of the pellet fuel used a sequence of thermal and mechanical treatments of the initial oxide powders. All pellet fabrication operations were done in stainless steel glove boxes with a controlled high purity argon atmosphere. Oxygen and moisture levels of less than 10 ppm were maintained in the glove boxes. Fig. 1 shows the process steps and gives a comparison of this method with the sphere-pac fuel production route.

Table 1
Sphere-pac fuel characteristics of AC-3 experiment

Fuel type	Sphere-pac average	Pellet average
Fissile composition		
^{235}U (at.%)	0.72	0.2
^{239}Pu (at.%)	88.20	87.08
^{240}Pu (at.%)	10.89	11.54
^{241}Pu (at.%)	0.68	1.1
Chemical composition		
Uranium (wt%)	73.00	75.06
Plutonium (wt%)	19.14	19.66
Thorium (wt%)	0.16	n.d.
Carbon (wt%)	4.93	4.99
Oxygen (wt%)	0.11	0.052
Sulpher (ppm)	1600	<5
Nitrogen (ppm)	85	92
Tungsten[a] (ppm)	360	<10
Silicon[b] (ppm)	23	<10
Chromium (ppm)	13	<5
Iron (ppm)	37	100
Nickel (ppm)	2	<5
Pin make up		
SPHERE size: large fraction/small fraction (μm)	790/70	
Averaged fuel density (g/cm^3)	13	11
Fuel loading per pin (large fraction + small fraction) (g)	407 + 135	534
Fuel smear density (%TD)	78.8–80.3	75.4–78.7
Concentration of secondary phase (vol.%)	4.5 MC_2	12.0 M_2C_3

[a] Crucible contamination (one batch excluded in average).
[b] Oil bath contamination (one batch excluded in average).

3. Sphere-pac and pellet pin design

For ease in comparing performance, the sphere-pac and pellet pins were structured as nearly identical as possible (Fig. 2). The sphere-pac pin layout therefore closely followed the US FFTF pellet design with identical geometry and cladding materials. The cladding, end-caps and wire wrap were made out of 20% cold worked titanium stabilized D9 stainless steel with 14% Cr, 15.5% Ni, 1.5% Mo, 2.1% Mn and 0.18% Ti [18]. The cladding had an outer diameter of 9.40 mm and a wall thickness of 0.51 mm. The total pin length was 2372 mm. The active fuel column had a length of 914 mm with its bottom approximately 200 mm above the pin bottom end. All pin axial elevation references in this report are related to this pin bottom end. Two depleted UC insulator pellets and a reflector bar were placed above and below the fuel column. The upper gas plenum contained a plenum spacer tube, a compression tube and close fitting molybdenum discs at each end of the fuel column to retain the fine micro-spheres (two differing design events for the pellet pins) and a tag gas capsule, containing a specific mixture of xenon and krypton isotopes unique for the AC-3 experiment. The pins were filled with high purity helium. Extensive filling trials with dummy materials were carried out to optimise the filling technique (using the method of fines infiltration after filling and compacting the coarse fractions) and to demonstrate

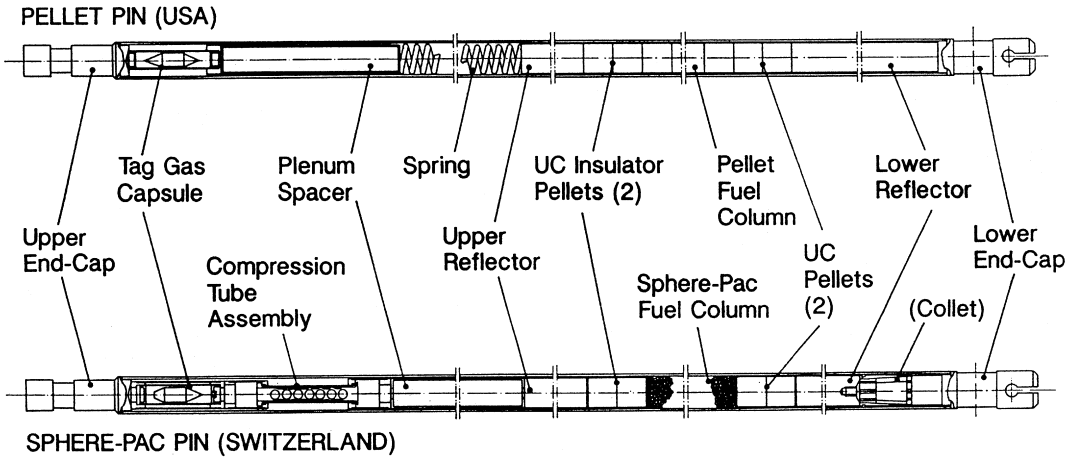

Fig. 2. Pin layout for sphere-pac and pellet pins.

consistent and flat axial density profiles for the fuel column by axial gamma scanning.

All fuel preparation-, characterization-, and pin filling work was performed under strict quality management and control to reach the FFTF quality requirements. A total of 27 sphere-pac pins were fabricated, including spare and archive pins. The fuel column smear density ranged from 78.8% to 80.3% theoretical density (Table 1).

The pellet pin design used was typical of the design of the FFTF driver fuel pins. Fuel pellets had a nominal length of 8.8 mm, a nominal diameter of 8.23 mm, thus providing a nominal fuel cladding diametral gap of 0.15 mm. A total of 77 pellet pins were fabricated including spare and archive pin. Each pin contained from 101 to 106 fuel pellets. The smear density of the fuel columns ranged from 75% to 78.8% theoretical density (TD).

4. Fuel bundle make up

25 of the PSI filled sphere-pac fuel pins were then shipped to Westinghouse, Hanford Cie. (WHC), where they were assembled with 76 LANL-pellet pins into the AC-3 FFTF fuel bundle. The ninety-one pins were mounted into a hexagonal duct (made of 20% cold worked D9 stainless steel) of a 3.65 m long assembly (Fig. 3). A helical wrap of D9 wire on each cladding tube provided

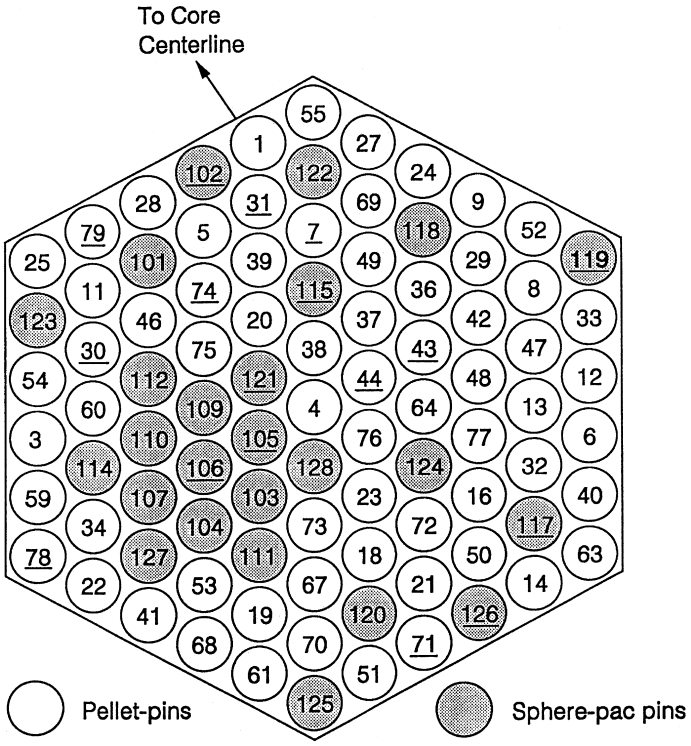

Fig. 3. Make up of the AC-3 fuel bundle.

pin-to-pin separation which created a flow path for the sodium.

5. FFTF irradiation

The AC-3 assembly was loaded into the FFTF fuel core in August 1986 in row 4. Irradiation began in September 1986, referred to as beginning of life (BOL), and was completed in October 1988, referred to as end of life (EOL). lt went through five reactor cycles, totalling 620.3 effective full power days (EFPD), reaching at peak power position of the pins a fast fluence of ~14E22 ncm^{-2}. A typical power history for a sphere-pac and a pellet pin is given in Fig. 4.

The nominal bulk sodium coolant inlet temperature was 360 °C. Calculations for nominal peak pin linear heat rates, coolant outlet temperatures and peak fast neutron fluxes were performed at WHC and reported for each individual pin for the beginning and end of each cycle, defined in units of EFPD.

Some of this basic data, together with pin fissile density data and information on the axial power distribution was input into the PSI codes F_AC3 and AC3_ASSY. These codes were used for calculating density-corrected linear powers, coolant temperatures, cladding surface temperatures and fast fluxes for any axial pin location and exposure time, as well as burn up and fast fluencies at EOL. The axial flux and power distribution applied in the code F_AC3 was derived from post-test measured ^{54}Mn gamma profiles. The polynomial and normalized fits to the ^{54}Mn gamma scans from several fuel pins showed almost no spread, indicating an undisturbed and uniform axial flux profile throughout the assembly. Although the activation product ^{54}Mn with its half life of 312 days started to saturate during the irradiation period of about two years, its axial distribution is considered to be also fairly representative for the time-averaged neutron flux profile in the AC-3 assembly. In the present report, calculated local pin specific flux and fluence, as well as linear power and burn up are therefore based upon this profile. Integrating the pin specific flux profile over the fuel length then delivers the normalized axial coolant temperature profile, shown in Fig. 5. With given sodium inlet- and outlet-temperatures, local coolant temperatures and power levels for individual pins could then be calculated by interpolation Fig. 6. Finally, the local outer cladding temperatures were derived from linear power, coolant temperature and appropriate heat transfer coefficients.

The mean linear pin power in the peak power plane (at 60 cm level) of the AC-3 assembly, averaged over all pins and over the total irradiation time, was calculated to be 66.1 kW/m. The corresponding mean cladding surface temperature was about 439 °C and 508 °C at the fuel column top end. The BOL- onditions for the highest power pins at peak power plane were 81.5 kW/m with a corresponding cladding surface temperature of 466 °C, corresponding to 558 °C at fuel top end. The irradiation conditions of individual pins obviously diverged considerably from these average data due to different pin fissile densities as well as reactor-specific neutron flux gradients and coolant flow distributions (Fig. 6).

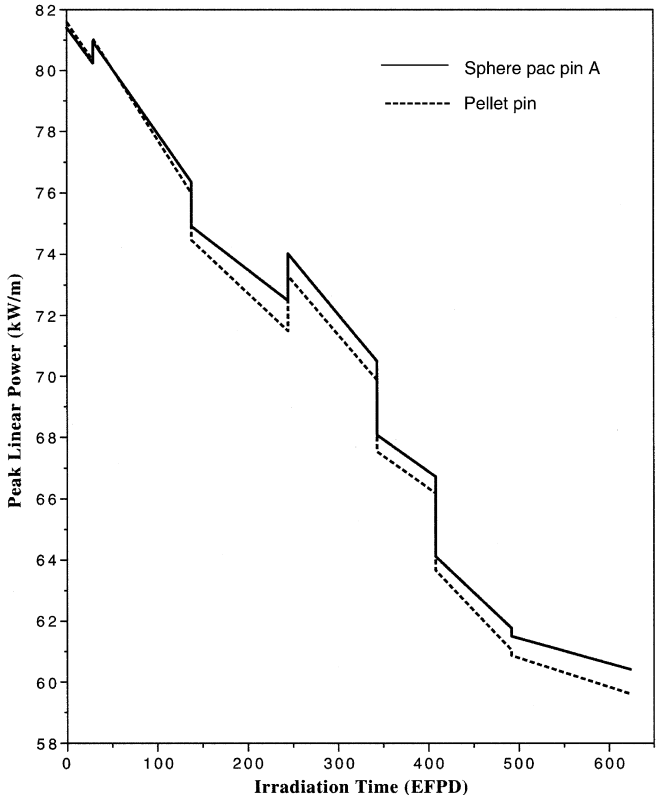

Fig. 4. Linear power history at peak power level for sphere-pac pin A and a comparable pellet pin.

6. Sphere-pac fuel PIE, expected and proven results compared to the pellet fuel

6.1. General overview

As stated above, the AC-3 bundle test consisted of ninety-one (U,Pu)C fuel pins with D9 stainless steel cladding. D9 is one of the well researched US candidate steels for its LMR program with delayed swelling compared to stainless steel 316L [18]. Sixty-six of them contained pellet fuel and the remaining 25 pins sphere-pac fuel. (The behaviour of the pellet pins will mainly be described in a later paper [19].) The nominal fuel design composition for pellet- and sphere-pac fuel was $(U_{0.8},Pu_{0.2})C$ with an equivalent carbon content[1] of ~5%.

Because fuel pins of the 'sphere-pac type' are not generally well known, an overview on some special features of this concept (as compared to the pellet concept) will first be given (the data being typical for the AC-3 carbide fuel):

[1] Defined as $C_{aeq} = C + 12/14\ N + 12/16\ O$.

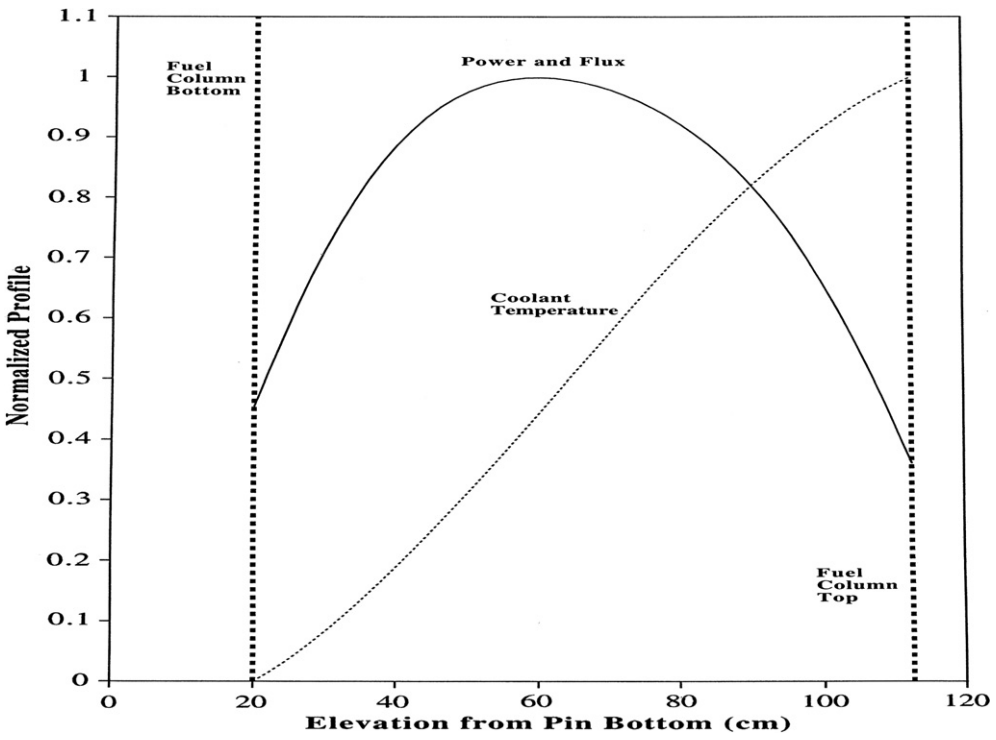

Fig. 5. Normalized power and coolant temperature profiles for the AC-3 fuel bundle calculated with PSI code 'F_AC3'.

- Instead of pellets fabricated to close geometrical tolerances, the pin is filled with spherical particles of two diametral fractions, produced by the described wet chemical process (highest fuel densities are reached with particle sizes about 10% and 0.9% of cladding inner diameter).
- In a pellet pin, the pellet 'inner porosity' (~20%) and the void provided by pellet-geometry (gas gap, chamfer, dishing), accounting for an 'outer porosity' of ~3% are the determining parameters for adjusting the required 'smear density' (77%). In a sphere-pac pin the relation of inner to other void is about reversed: particle 'inner porosity' is very low (~3%) and 'outer porosity' (the interstices between particles) relatively high (~18%), resulting however in a similar 'smear density' (~79% for the AC-3 experiment).

The BOL fuel temperature in pellet pins is determined by the thermal conductivity of the bulk fuel and the gap conductance. In sphere-pac pins, fuel temperature is almost entirely determined by the 'macroscopic conductivity' of the particle bed, which was calculated in special sphere-pac modelling codes. Correspondingly the BOL radial temperature profiles in pellet and sphere-pac pins are quite different: Pellet pins show a relatively high temperature jump in the gas gap, but moderate temperature gradients within the pellet, while in sphere-pac pins (with no gas gap) no temperature jump at the fuel–clad interface, but a higher temperature gradient within the bed of spheres is expected.

Fuel restructuring at BOL is also quite different: Pellets usually crack and rearrange during the first start up (pellet relocation). Although high temperatures and burn up tend to heal fine cracks, wide cracks stay open until the occurrence of fuel clad mechanical interaction (FCMI) and often throughout life. A fresh sphere-pac fuel bed obviously cannot crack. Already with the first start up, sintering mechanisms start to convert the initially lose bed of particles towards a finally porous, pellet-like structure. The degree of this restructuring strongly depends on temperature, but also on mechanical stress. It is strongest in the fuel centre region and decreases towards the outer fuel rim (Fig. 7). Due to this ongoing 'pin conditioning', significant fuel cracking does not occur in sphere-pac pins under normal operating conditions.

Well known for both pin types are of course the 'cooling down cracks' (especially those from final shut down). These cracks due to thermal contraction of the fuel can be observed in PIE ceramography but are of little significance for the pin operating behaviour.

There are also basic differences in the fuel clad mechanical interaction (FCMI). In pellet pins, FCMI is delayed until the diameter increase due to thermal expansion and fuel swelling has used up the 'outer porosity' (~3%) provided by the fuel–clad gap. Then the FCMI rises strongly, because the compressive load required to reduce the pellet 'inner porosity' (~20%) is relatively high. Frictional forces at the pellet-cladding interface then start to retain and finally disable the axial expansion of the fuel column into the upper gas plenum.

In sphere-pac pins FCMI already starts at BOL since the fuel is in mechanical contact with the cladding. Axial expansion of the fuel column relative to the cladding is gen-

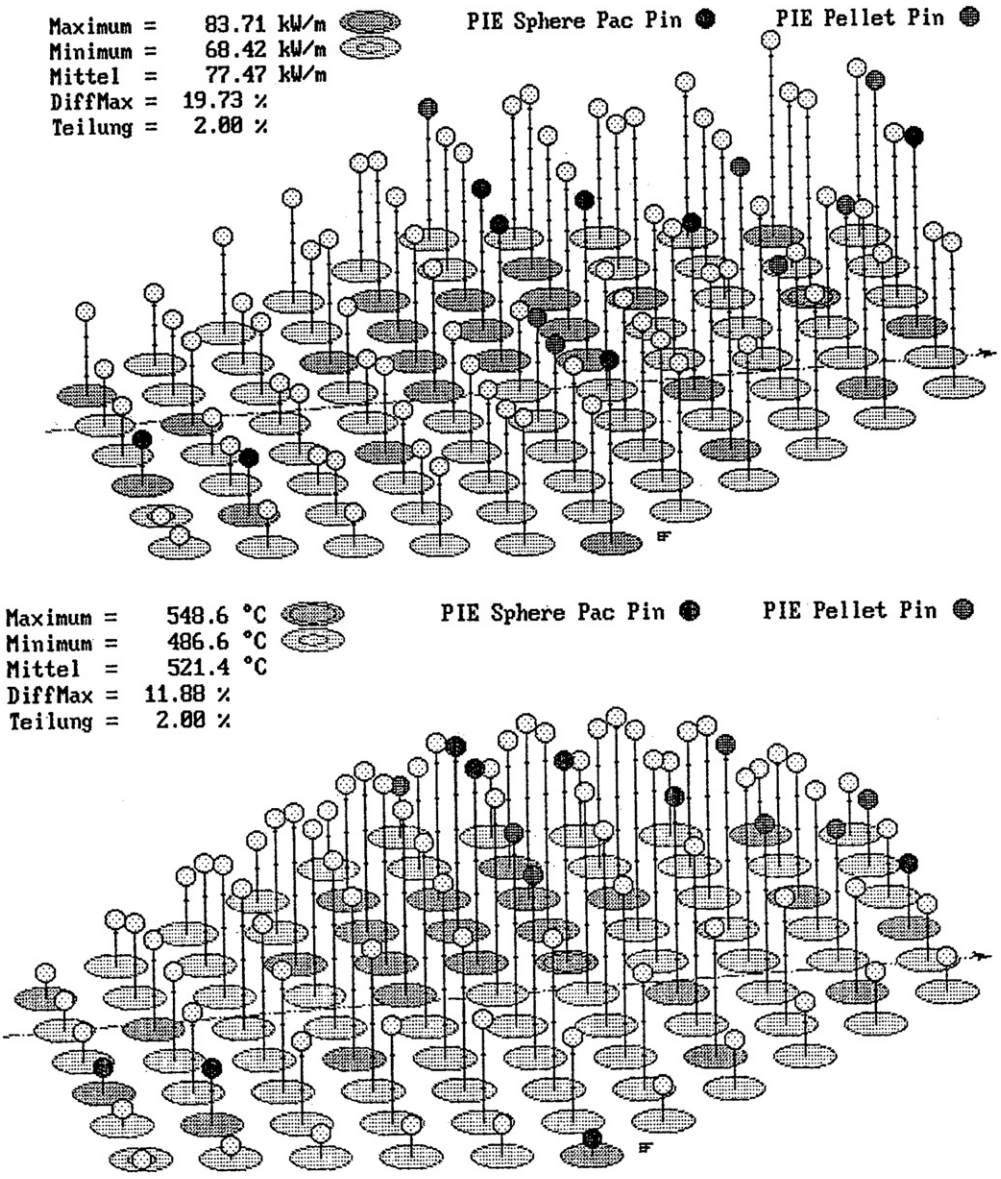

Fig. 6. Overview of peak linear powers (top) and sodium outlet temperatures (bottom) for the AC-3 bundle at begin of irradiation, calculated with PSI code 'AC3_ASSY'.

erally suppressed by friction in the fuel–cladding interface. Any (positive) differential expansion between fuel and cladding due to thermal expansion or swelling has thus to be taken up by a reduction of the fuel outer porosity (i.e. the interstices between particles) and an increase of the cladding diameter. Thanks to the inherent 'softness' of a sphere-pac bed (basically governed by the size of the contact areas of touching spheres), the compressive load required to reduce the 'outer porosity' (18%) is initially rather low and rises only slowly.

Summarizing: FCMI in sphere-pac pins already starts at BOL but then rises only at a moderate rate. FCMI in pellet pins is time delayed, but then rises at a far steeper rate. Thus up to a certain time or burn up, pellet pins will develop a lower FCMI than sphere-pac pins. Above this limit, the situation is expected to be reversed.

6.2. Sphere-pac fuel behaviour modelling

To quantitatively investigate and estimate some of the specific effects in the sphere-pac irradiation behaviour, the code SPHERE was developed at PSI [20,21]. It takes into account the pin power, coolant temperature, mechanical pressure in the fuel bed and material properties, and calculates the degree of restructuring, the porosity, the macroscopic thermal conductivity of the particle bed, the fuel and cladding temperatures and the fission gas release. As mentioned above, the characteristic and most significant phenomenon in sphere-pac fuel is its restructuring, i.e. the successive transformation of the initial bed of individual micro-spheres into a sintered porous body. In SPHERE this is modelled by a gradual build up of 'necks' between adjacent spheres, thus increasing their contact area. This

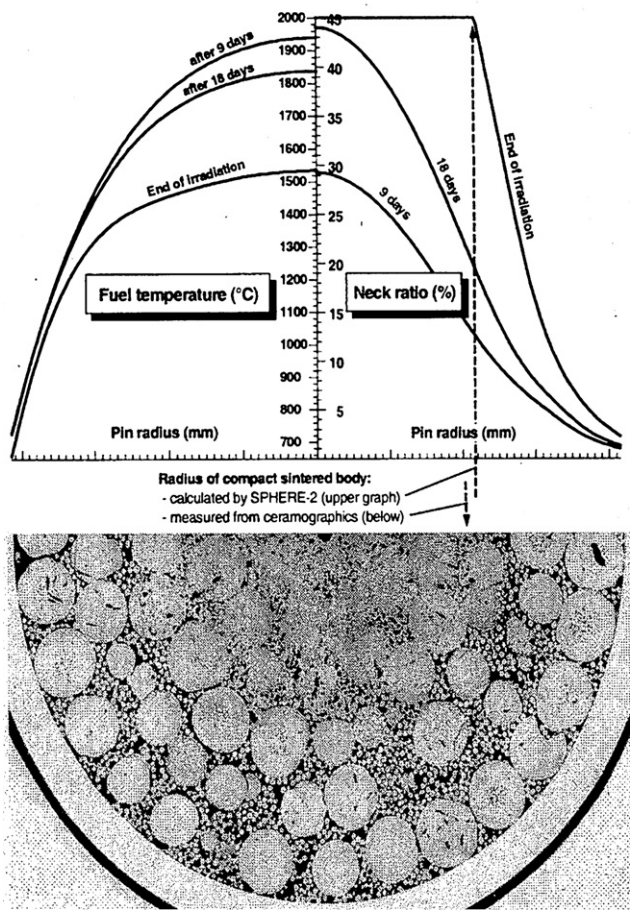

Fig. 7. Fuel temperatures and neck ratio (degree of restructuring) as calculated with PSI code 'SPHERE' for peak power cross section of pin A (top) and ceramographic transverse cross section of the same pin at the same axial position.

obviously improves the heat transport in the fuel bed and reduces the fuel centre temperature.

For calculating the development of such necks, SPHERE considers mass diffusion mechanisms (such as surface-, grain boundary-, volume diffusion, evaporation–condensation) as well as deformation processes due to mechanical stresses, any of which can be the dominating mechanism, depending on the local irradiation conditions (see also Fig. 8). As it turns out, the dimensionless 'neck ratio' (defined as D_{neck}/D_{sphere}), rather than the absolute neck diameter is the important factor determining the heat transport in such a structure. It is therefore used in SPHERE as the characteristic parameter describing the degree of restructuring.

From previous modelling calculations it was found that the calculated conductivity of a fuel particle bed reaches that of a solid body of equivalent porosity, when the neck ratio approaches about 0.45. Thus, where ever this value is reached, the fuel is considered as fully sintered and further neck growth is stopped. The corresponding radial position in the fuel cross section is called 'sinter radius'. It separates the fuel cross section in a partly sintered outer ring, and a fully sintered inner region, which from now on is treated as a porous 'pellet-like' body (Fig. 7).

6.3. PIE proof of sphere-pac fuel irradiation behaviour

Somewhat unconventionally the experimental PIE findings of the AC-3 test, analysed at WHC, Richland, INL, Idaho and ANL, Illinois, shall be discussed from inside out. We start with the (sphere-pac) fuel microstructure and the fuel behaviour which largely dictates the cladding behaviour and which was qualitatively described before. Then we describe the actual cladding behaviour and eventually compare the results with the pellet pin behaviour.

Eight sphere-pac fuel pins and 7 pellet pins were selected for various reasons to undergo detailed NDT and DT-characterization, see Table 2. As sphere-pac pin A with initial linear power and clad surface temperature of 81.4 kW/m and 465 °C at peak power plane and burn up of 8.34 at.% was also modelled with SPHERE, the PIE results shall focus mainly on this pin, while for generalized PIE information the individual results of all analysed pins are averaged.

6.3.1. Fuel temperatures, restructuring, swelling, fission product migration and gas release

According to SPHERE calculations, the fuel centre temperatures in sphere-pac pins were highest at BOL, reaching about 1940 °C at 81.4 kW/m in the peak power plane of pin A (Fig. 8). As expected, restructuring was then most pronounced and reduced the fuel centre temperature within days by some 250 °C. The further drop of centre temperatures to finally about 1550 °C at EOL mainly reflects the drop in the linear power to ~60 kW/m (Fig. 4). The sinter radius at EOL for this cross section, as calculated by SPHERE, reaches about 52% (Fig. 9). Its growth rate is also shown in this figure, together with the growth of sinter radii in other cross sections above and below the peak power level.

From the ceramographic transverse cross section in the peak power plane of pin A (Fig. 7) strong restructuring is evident. In the pin centre region the identity of small and large spheres is almost completely lost. Indicated in the figure are also the sinter radii as estimated with SPHERE calculations (52%), and as visually derived from ceramography.

The fully restructured area inside the sinter radius contains pores as large as the fuel grains and reveals the early stage in the development of a central hole. It should however be realized that (in contrast to pellet fuel) most of the pores in the restructured sphere-pac fuel were transformed from the initially open void provided by the interstices in the sphere-pac fuel. This is also why the AC-3 sphere-pac fuel, despite the relatively high linear power and burn up, did not show unfavourable total geometrical fuel swelling data (Table 2), which, according to many authors can reach very high values (without restraint $\geqslant 1.5\%\ \Delta V/V$ per 1% FIMA burn up) in carbide fuels [2,13].

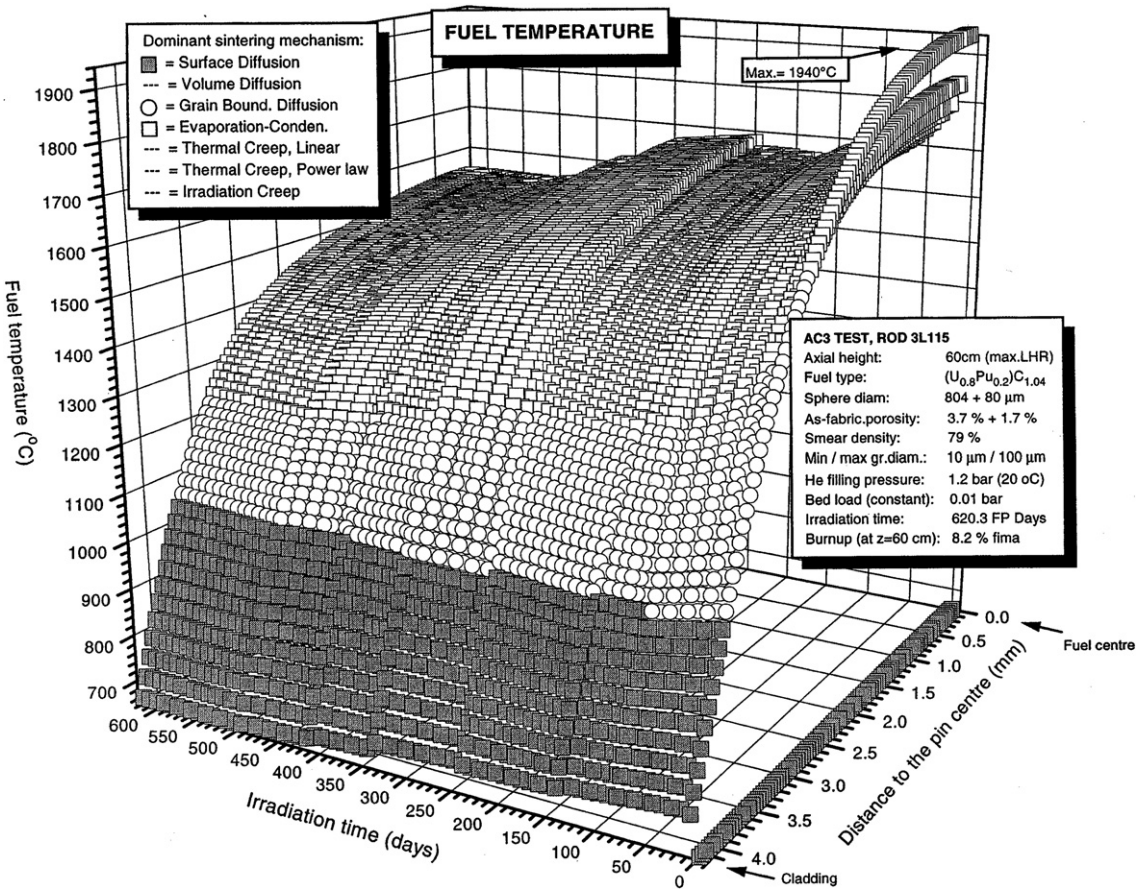

Fig. 8. Fuel temperatures in sphere-pac pin A in function of fuel radial position and irradiation time, calculated with PSI code 'SPHERE'.

Table 2
PIE results of sphere pac pin A and averaged results of 7 pellet pins and 8 sphere pac pins

Pin type and identity	Operating conditions in peak power plane				PIE results			
	Linear power		Temperature clad surface	Burn up	Length increase	Pin diameter increase	Fuel swelling[a]	Fission gas release
	At BOL (kW/m)	Time averaged (kW/m)	At BOL (°C)	At EOL (at.%)	Fuel column total $\Delta L/L$ (%)	Fuel column peak $\Delta D/D$ (%)	Fuel column total $\Delta V/V$ (%)	Fuel column total (%)
Average of 7 pellet pins	79.3	67.5	456	8.28	1.33	1.70	3.44	7.75
Sphere-pac pin A	81.4	69.9	465	8.34	0.93	2.10	4.00	4.88
Average of eight sphere-pac pins	79.0	67.7	446	8.08	0.84	1.90	3.71	4.76

[a] As defined in Section 6.3.1.

In order to compare the swelling of the sphere-pac fuel with the pellet fuel in the AC-3 experiment, the total geometrical fuel swelling here is defined as the relative difference of the fuel volume at BOL, to the volume occupied at EOL, the former being given by the initial fuel stack length and cladding inner diameter, the latter being extracted from neutron radiographic fuel column height and cladding profilometry measurements. The fuel volume increase in sphere-pac pins was 3.71% $\Delta V/V$, thus slightly higher than for the AC-3 pellet fuel with 3.44% $\Delta V/V$. This difference is partly due to the higher cladding strain at both fuel column ends of the sphere-pac pins (as discussed in Section 6.3.2), but also related to the ~2% higher smear density of the sphere-pac pins, corresponding to ~10% less free volume available to take up swelling. With the mean burn up being about 6.75 at.%, the burn up specific sphere-pac volumetric swelling rate (as defined above) becomes approximately 0.55% $\Delta V/V$ per 1% FIMA. Due to the different swelling definitions and the lack of measured, density based PIE swelling data, a direct comparison

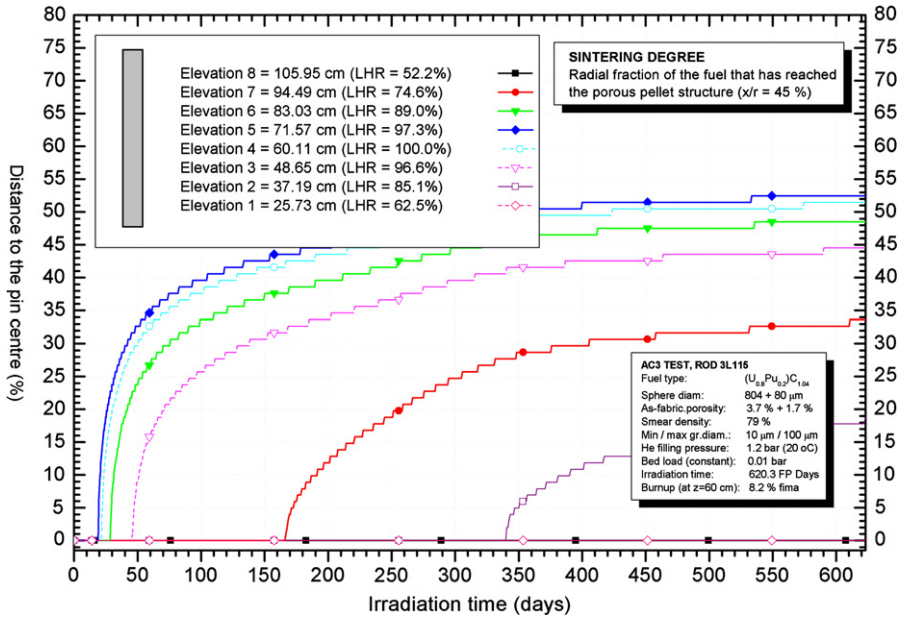

Fig. 9. Development of sinter radius (necking 45%) in sphere-pac pin A in function of axial elevation and irradiation time, calculated with PSI code 'SPHERE'.

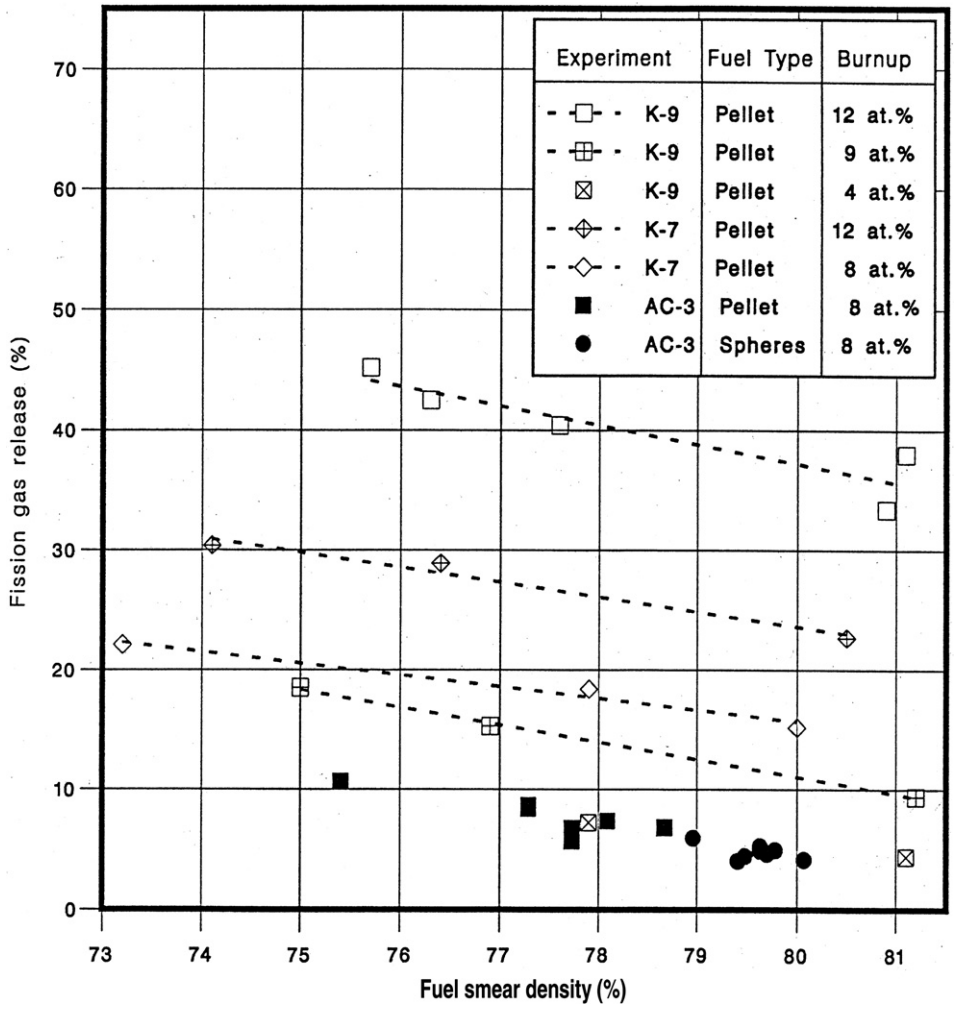

Fig. 10. Fission gas release in function of fuel smear densities. Results of the AC-3 experiment compared to earlier EBR-2 data.

with values from other pellet fuel irradiations is however not possible.

With the reasonably low fuel swelling data it could have been assumed that the fission gas release of the helium bonded sphere-pac fuel, with relatively high central temperatures (Figs. 7 and 8) and an assumed large interconnected void system, might be rather high. But the average value of 4.76% measured from eight sphere-pac pins (Table 2) was quite low and was even lower than the 7.75% average value for the pellet pins, despite the fact that the fuel centre temperature of the sphere-pac fuel was estimated higher than for the pellet pins. It has to be assumed therefore that the sphere-pac fuel microstructure revealed a larger amount of open porosity. The AC-3 fission gas release values in total were also lower than earlier EBR-II data, all values revealing a general tendency of decreasing FGR with increasing fuel smear density (leading to higher thermal conductivities and lower temperatures) (Fig. 10).

Another information about fuel temperatures stems from Cs fission product profiling as indicated in Fig. 11 with the axial distribution of ^{134}Cs and ^{137}Cs. The ^{137}Cs activity profiles of all the sphere-pac pins were quite similar to the burn up (i.e. ^{54}Mn-) profile, they gave no evidence for a significant axial migration, perhaps with the exception of some accumulation in the pin bottom region. The general shape of the ^{134}Cs profiles however differs from the burn up profile in two respects: It shows a more pronounced buckling in the pin peak power region and a distinct peak at the bottom end of the fuel column. The accumulation of ^{134}Cs at the fuel column bottom is likely to stem from the precursor fission isobar nuclides ^{133}I and ^{133}Xe, which may have migrated axially, decaying to ^{133}Cs which then is activated to ^{134}Cs. From this it can be concluded that cesium retention in sphere-pac fuel was quite high.

6.3.2. Cladding-carburization, -creep and -growth

The sphere-pac fuel with some 4-5% of UC_2 equivalent could have revealed some cladding carburization; as such damage has been seen elsewhere. However there was only limited chemical interaction of the cladding in the AC-3 pins. Metallographic examinations after etching revealed a reaction Iayer on the inside surface of the cladding of approximately 3 μm. This layer was uniform around the inner circumference of the cladding on all pins. The depth of the observed reaction layers was less than 1% of the as-built cladding wall thickness and indicates minimal threat to the containment provided by the cladding.

As discussed in Section 6.1, fuel–cladding-mechanical-interaction (FCMI) in sphere-pac fuel starts from the very beginning of the irradiation as there is no pellet cladding gap available. Fig. 12 shows the result of the axial diameter

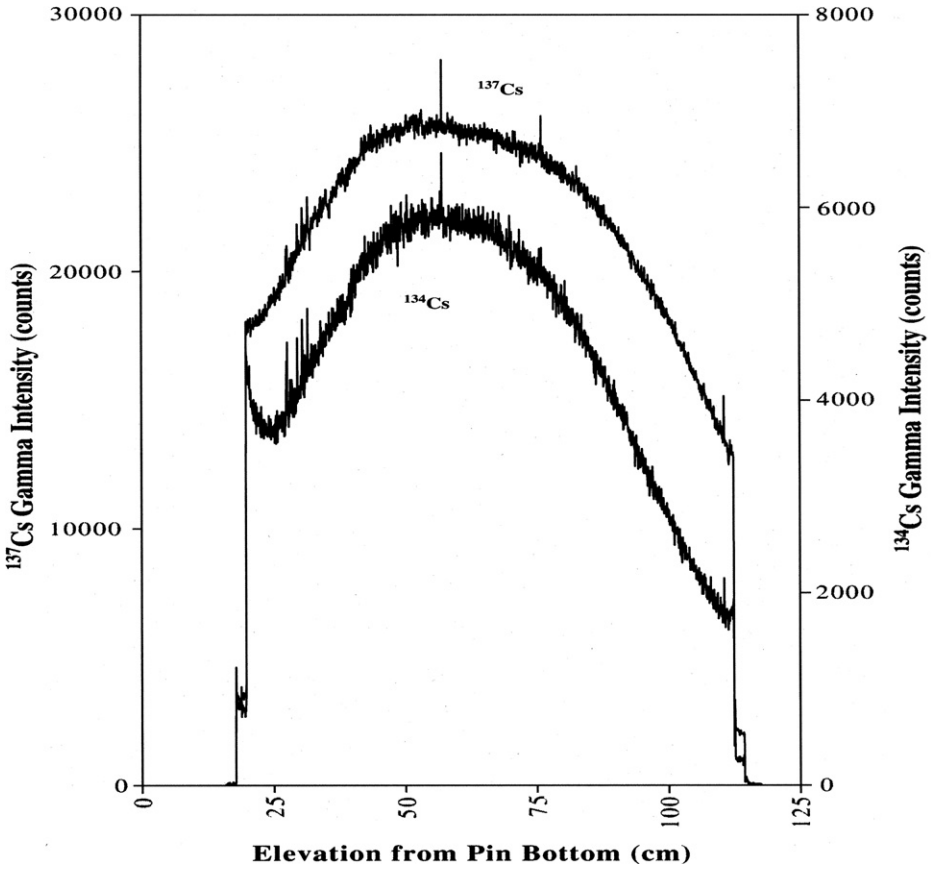

Fig. 11. Axial gamma scanning results with distribution of ^{134}Cs and ^{137}Cs in sphere-pac pin A, indicating no diffusion of ^{137}Cs and diffusion of the ^{134}Cs precursors ^{133}I and ^{133}Xe.

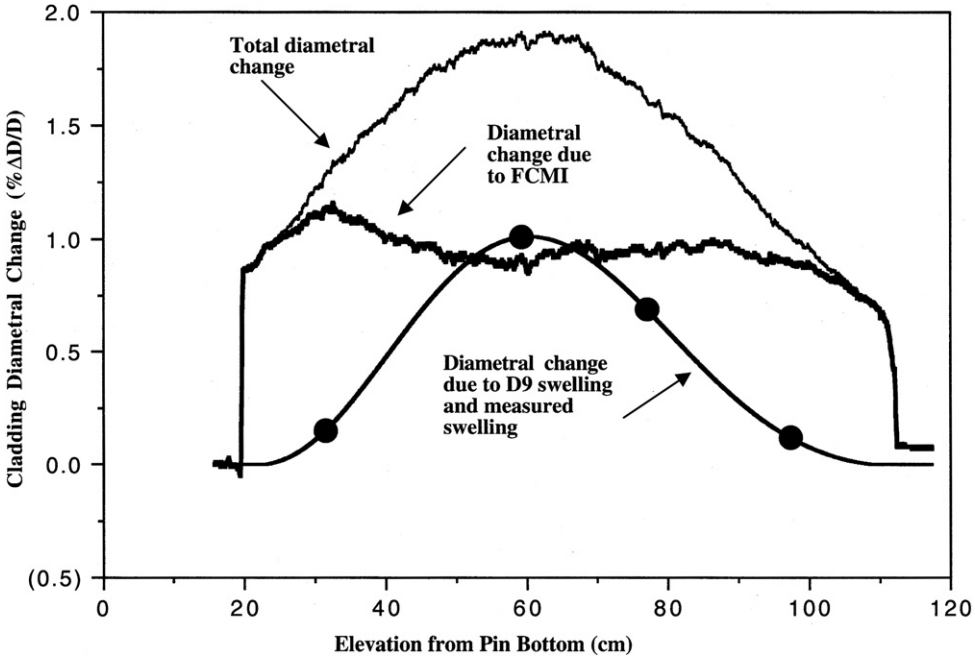

Fig. 12. Axial variation of cladding diameter change for sphere-pac pin B indicating also the measured cladding swelling.

profilometry of sphere-pac pin B (typical for all sphere-pac pins). Shown are the total diametral increase of the cladding (as measured), the diametral increase due to swelling of the cladding material (calculated curve based on individual measured (●) points), and finally their difference, assumed to account for cladding creep due to FCMI. Considering the distinct power and temperature profiles (Fig. 5), this is surprisingly constant over the full fuel column length. In the peak power area and thus high temperature region, a large part of the fuel swelling is taken up by the high fuel compressibility, while in the lower powered, cooler fuel end regions, the sphere-pac fuel remains somewhat more rigid, thus increasing the FCMI. The abrupt drop at the fuel column ends marks the position of the insulator pellets with still open gas gaps, preventing any mechanical interaction with the cladding.

In pellet pins (not shown here) the cross over from the fuel column to the insulator pellets is smoother, since at EOL the gas gaps in these fuel regions were not (or only just about) closed. Thus, no FCMI occurred here. However, further irradiation would also have closed these gas gaps, leading to similar steps in the clad diameter profile as observed at the sphere-pac pins.

The maximal FCMI induced diametral cladding creep was around of 0.8% $\Delta D/D$ for both pin types. Single deviations from this value in the order of $\pm 0.1\%$ can be explained by differences in smear density, linear power and burn-up.

Similarly, some differences in axial strain were found. While in pellet pins the whole stack of pellets is free to axially expand until FCMI starts to hinder this, it is essentially not possible in sphere-pac pins. Here any significant axial expansion of the fuel particle bed relative to the cladding tube is blocked-up by friction in the fuel–cladding interface. PIE length measurements and neutron radiography confirm this insofar as the average axial growth of sphere-pac pins (8.13 mm) corresponded pretty much to the average growth of the she sphere-pac fuel columns (7.65 mm), while the pellet pins with essentially the same change in total pin length showed an average fuel stack growth of about 12 mm, or 4 mm relative to the cladding.

7. Summary

91 helium bonded mixed carbide fuel pins with pellet and sphere-pac fuel, clad in D9 stainless steel, were irradiated in FFTF to 8.5 at.% peak burn up and $1.47\ 10^{23}\ \mathrm{ncm}^{-2}$ peak fast neutron fluence. The time averaged linear power at the peak power plane was around 66 kW/m and the corresponding cladding surface temperature about 440 °C. The only planned and well defined difference between pellet and sphere-pac fuel (apart from the basically different geometrical structure and the related production procedure) concerned their range of the smear density: Approximately 75.4% to 78.7%TD in pellet pins, and 78.8 to 80.3%TD in sphere-pac pins.

During the 630 equivalent full power days of reactor operation, neither of the 66 pellet pins nor the 25 sphere-pac pins failed. PIE was carried out on 7 pellet and eight sphere-pac pins. The results and conclusions are summarized below (data given are averages for the related pin types):

- Peak cladding diametral strain was about 0.16 mm (1.7%) for pellet and 0.18 mm (1.9%) for sphere-pac pins. This difference is most likely related to the 2% higher smear density of the sphere-pac fuel. The axial strain is about 8.1 mm for both pin types.

- The volumetric fuel swelling rate (in this report based on initial cladding inner diameter and fuel column length) for pellet and sphere-pac fuel was 0.51% and 0.55% volume per 1% average burn up increase. Taking into account the 2% higher smear densities of the sphere-pac pins, this again is not considered as a pin type specific difference.
- Peak volumetric swelling of the D9 cladding was around 3% for 1.4 10^{23} n/cm^2 and 480 °C.
- Fission gas release in general was relatively low when compared to EBR-ll data. Significantly higher values have been measured in pellet pins (7.8%) than in sphere-pac pins (4.8%). This difference is most likely related to a basically different micro structure of these two fuel types. We assume closed porosity in the large spheres of the sphere-pac fuel vs. open porosity in the pellet fuel which might be further analysed.
- Fuel restructuring in the peak power plane of sphere-pac pins was evident. In the fuel centre the initial matrix of coarse and fine spheres was almost fully converted into a recrystallized porous structure. There is in one case even evidence for the formation of a central hole. Only minor cracking, preferably in circumferential direction, occurred during cooling down at EOL. The restructuring was expected and modelled with the PSI fuel code SPHERE.
- Fission product axial distribution was analysed by axial gamma scanning. Among the fission products investigated (Ce, Rh, Sb, Zr, Nb and Cs), only the cesium isotope 134 showed significant axial redistribution in the sphere-pac pin concept.
- In both pellet and sphere-pac pins, fuel cladding chemical interaction was very limited with an interaction layer of 2–3 μm, observed in the peak power planes. Metallography and micro-hardness measurements indicated no evidence for significant cladding carbon uptake.

The irradiation behaviour of both pellet- and sphere-pac pins was excellent and quite comparable, besides some marked differences concerning detailed aspects as listed above. Stronger differences and advantages for the sphere-pac pin concept might be expected and found in comparative tests at higher ratings and to a higher burn up applying also a further developed sphere-pac pin design. The improvements would consist in (a) placing the fissile material only in the large high density spheres and (b) replacing the insulator pellets against an insulator sphere column of equal height. This would also result in simplifications in the fabrication process not only for carbides but also for carbonitrides which have been fabricated in a similar manner [22].

The AC-3 irradiation test program was a cooperative effort between US and Swiss nuclear fuel researchers. The interaction between the staff of LANL, PSI, WHC and ANL provided a valuable exchange of ideas, issues and concerns which resulted in a worthwhile evaluation of two candidate FBR-fuels. The authors would like to thank all staff members in the mentioned institutes, be it on the technical/engineering level or in the administrative, directing level. The program would not have been possible and successful without all clearly directed and combined efforts.

References

[1] R.B. Matthew, R.J. Herbst, Nucl. Technol. 63 (1983).
[2] M. Fromont, J. Lamontagne, M. Asou, I. Aubrun, in: Proceedings of the Global 2005, Tsukuba, Japan.
[3] T.S. Subramanian, A milestone at Kalpakkam <http://www.hindu.-com/2005/06/12/stories/2005061203451200.htm>.
[4] K. Ananthasivan, S. Anthonysamy, V. Chandramouli, I. Kaliappan, P. Rao, J. Nucl. Mater. 228 (1996) 18.
[5] G. Ledergerber, R. Herbst, H.U. Zwicky, H. Kutter, P. Fischer, J. Nucl. Mater. 153 (1988) 189.
[6] T.W. Latimer et al., The K4 Test: Sodium-Bonded Uranium–Plutonium Carbide and Nitride Fuel Pins Irradiated to 9-at% Burn Up in EBR.II, LA-9482, June 1982.
[7] R.L. Petty et al., The K9/K10 Test: Irradiation Behaviour of Uranium–Plutonium Carbide Fuel Pins Operated at Moderate Power and High Cladding Temperatures, LA-10204, March 1985.
[8] R.L. Petty et al., The K7 Test: Irradiation Behaviour of Uranium–Plutonium Carbide Fuel Pins at Burn Ups to 16–17 at% at High Power in EBR-II LA 10403, January 1986.
[9] L. Smith et al., The post irradiation examination of a sphere-pac (U,Pu)C fuel pin irradiated in the BR-2 reactor (MFBS-7 experiment), EIR-376, 1979.
[10] K Bischoff, et al, Performance of a Sphere-pac Mixed Carbide Fuel Pin Irradiated in the Dounreay Fast Reactor (DFR 527/1 Experiment), EIR-415, October 1980.
[11] G. Bart et al., The post irradiation Examination of Four Sphere-pac (U,Pu)C Fuel Pins, Irradiated in the Harwell DIDO Reactor, EIR-450, 1987.
[12] R.E. Mason, C.W. Hoth, R.W. Stratton, F.B. Botta, Trans. Am. Nucl. Soc. 66 (1992) 215.
[13] H.J. Matzke, Science of Advanced LMFBR fuels, North-Holland Physics Publishing, 1986, ISBN: 0 444 86997 2 (US).
[14] C. Ganguly, P.V. Hegde, J. Sol–Gel Sci. Technol. 9 (1997) 285.
[15] G. Ledergerber, F. Ingold, R.W. Stratton, H.P. Alder, Nucl. Technol. 114 (1996) 194.
[16] M. Jolkkonen, M. Streit, J. Wallenius, J. Nucl. Sci. Technol. 41 (2004) 457.
[17] R.W. Stratton, G. Ledergerber, F. Ingold, T.W. Latimer, K.M. Chidester, J. Nucl. Mater. 204 (1993) 39.
[18] B.J. Makenas, S.A. Chastin, B.C. Gneiting, Dimensional Changes in FFTF Austenitic Cladding and Ducts WHC-SA-0933-FP, 1990.
[19] R.E. Mason, private communication.
[20] H. Wallin, L.Å. Nordström, C. Hellwig, in: Proceedings of the IAEA TCM on Nuclear Fuel Behaviour Modelling at High Burnup, Windermere, UK, 19–23 June 2000.
[21] H. Wallin, L.Å. Nordström, C. Hellwig, in: Proceedings of the IAEA/NEA/CEA International Seminar on Fission Gas Behaviour in Water Reactor Fuels, Cadarache (F), September 2000.
[22] G. Ledergerber, Z. Kopajtic, F. Ingold, R.W. Stratton, J. Nucl. Mater. 188 (1992) 28.